Springer

Journal of Mechanical Science and Technology 23 (2009) 1~7

Journal of Mechanical Science and Technology

www.springerlink.com/content/1738-494x
DOI 10.1007/s12206-008-0919-2

Dynamic propagation of a finite eccentric crack in a functionally graded piezoelectric ceramic strip †

Jeong Woo Shin*, Tae-Uk Kim, Sung Joon Kim and In Hee Hwang

Korea Aerospace Research Institute, 45 Eoeun-Dong, YouSeong-Gu, Daejeon, 305-333, Korea

(Manuscript Received April 5, 2007; Revised June 15, 2008; Accepted September 17, 2008)

Abstract

The dynamic propagation of an eccentric Griffith crack in a functionally graded piezoelectric ceramic strip under anti-plane shear is analyzed using the integral transform method. A constant velocity Yoffe-type moving crack is considered. Fourier transform is used to reduce the problem to a pair of dual integral equations, which is then expressed in a Fredholm integral equation of the second kind. We assume that the properties of the functionally graded piezoelectric material vary continuously along the thickness. The impermeable crack boundary condition is adopted. Numerical values on the dynamic stress intensity factors are presented for the functionally graded piezoelectric material to show the dependence of the gradient of material properties, crack moving velocity, and eccentricity. The dynamic stress intensity factors of a moving crack in functionally graded piezoelectric material increases when the crack moving velocity, eccentricity of crack location, material property gradient, and crack length increase.

Keywords: DSIF (dynamic stress intensity factor); Eccentric; FGM (functionally graded material); Moving crack; Piezoelectric

1. Introduction

Piezoelectric ceramic materials have recently attracted extensive attention due to their application in smart sensors and actuators. When piezoelectric ceramics are subjected to mechanical and electrical stresses in service, the initiation and propagation of cracks may result in the failure of these materials. To prevent failure during service and to obtain the reliable service lifetime of piezoelectric components, the fracture mechanics of piezoelectric ceramics have been given more attention in recent years. Most of the research have examined homogeneous piezoelectric materials. Recently, a few fracture mechanics research on functionally graded piezoelectric material (FGPM) have been presented. Li and Weng [1] studied the problem of a finite crack in a strip of FGPM. Functionally graded piezoelectric strip with eccentric crack under anti-plane shear was analyzed by Shin and Kim [2]. Shin et al. [3] analyzed the dynamic response of an eccentric crack in functionally graded piezoelectric ceramic strip under anti-plane shear impact loading. The dynamic behavior of a moving central crack in FGPM was studied. Jin and Zhong [4] examined a moving mode-III crack in FGPM. The propagation of an anti-plane moving crack in a functionally graded piezoelectric strip was studied by Jin et al. [5]. Kwon [6] analyzed the dynamic propagation of an anti-plane shear crack in a functionally graded piezoelectric strip. The problem of a moving mode-III crack in a functionally graded piezoelectric strip was discussed by Hu and Zhong [7].

In this paper, we study the problem of a moving eccentric crack off the center line in a functionally graded piezoelectric ceramic strip under anti-plane shear and in-plane electric loading. The Yoffe-type model for crack propagation is adopted. We assume that the properties of the functionally graded piezo-

† This paper was recommended for publication in revised form by Associate Editor Hyeon Gyu Beom

*Corresponding author. Tel.: +82 42 860 2026, Fax.: +82 42 860 2006
E-mail address: jeongdal@kari.re.kr

electric ceramic strip vary continuously along the thickness. The impermeable crack boundary condition is adopted (Shin and Kim [2]; Shin et al. [3]). Fourier transform is used to reduce the problem to a pair of dual integral equations, which is then expressed in a Fredholm integral equation of the second kind. Numerical results of the dynamic stress intensity factor are presented graphically to show the dependence of the gradient of material properties, crack moving velocity, and eccentricity.

2. Problem statement and formulation

Consider a functionally graded piezoelectric body in the form of an infinitely long strip containing a finite eccentric crack subjected to mechanical and electric loadings as shown in Fig. 1. The cartesian coordinates (X,Y,Z) are fixed for the reference. The piezoelectric ceramic strip poled with Z-axis occupies the region $(-\infty < X < \infty, -h_2 \le Y \le h_1, 2h = h_1 + h_2)$ and is thick enough in the Z-direction to allow a state of anti-plane shear. For convenience, we assume that the upper ($Y \ge 0$, thickness h_1) and lower ($Y \le 0$, thickness h_1) regions of the strip cracked with the eccentricity "e" off the center line have different thicknesses but consist the same functionally graded materials. The crack is situated along the virtual interface line ($-a \le X \le a,\ Y = 0$). Due to the symmetry in geometry and loading, it is sufficient to consider the right-hand half body only.

We assume that the properties of the functionally graded piezoelectric ceramic strip vary continuously along the thickness. They are simplified as follows (Erdogan [8]):

$$c_{44} = c_{44}^0 e^{\beta Y} \tag{1}$$

$$d_{11} = d_{11}^0 e^{\beta Y} \tag{2}$$

$$e_{15} = e_{15}^0 e^{\beta Y} \tag{3}$$

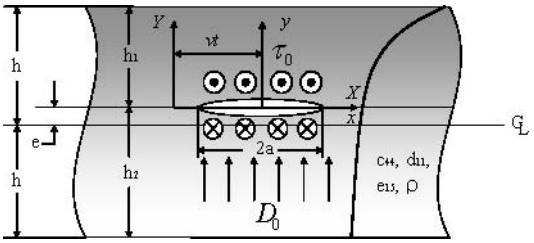

Fig. 1. A constant moving eccentric crack in a functionally graded piezoelectric strip.

$$\rho = \rho^0 e^{\beta Y} \tag{4}$$

where c_{44}, d_{11}, e_{15}, and ρ are the elastic modulus, dielectric permittivity, piezoelectric constant, and material density, respectively. c_{44}^0, d_{11}^0, e_{15}^0, and ρ^0 are the material properties at $Y = 0$, and β is the non-homogeneous material constant.

The piezoelectric boundary value problem is simplified considerably if we consider only the out-of-plane displacement and the in-plane electric fields such that

$$u_{Xi} = u_{Yi} = 0\ ,\ u_{Zi} = w_i(X,Y,t) \tag{5}$$

$$E_{Xi} = E_{Xi}(X,Y,t),\ E_{Yi} = E_{Yi}(X,Y,t),\ E_{Zi} = 0 \tag{6}$$

where u_{ki} and E_{ki} ($k = X,Y,Z$) are the displacements and electric fields, respectively. Subscript i ($i = 1,2$) stands for the upper and lower regions, respectively.

In this case, the constitutive relations become

$$\sigma_{Zji}(X,Y,t) = c_{44} w_{i,j} + e_{15}\phi_{i,j} \tag{7}$$

$$D_{ji}(X,Y,t) = e_{15} w_{i,j} - d_{11}\phi_{i,j} \tag{8}$$

where σ_{Zji}, D_{ji}, ($j = X,Y$), and ϕ_i are the stress components, electric displacements, and electric potential, respectively.

The dynamic anti-plane governing equations for FGPM are simplified to

$$c_{44}\nabla^2 w_i + e_{15}\nabla^2\phi_i + \beta\left(c_{44}\frac{\partial w_i}{\partial Y} + e_{15}\frac{\partial \phi_i}{\partial Y}\right) = \rho\frac{\partial^2 w_i}{\partial t^2} \tag{9}$$

$$e_{15}\nabla^2 w_i - d_{11}\nabla^2\phi_i + \beta\left(e_{15}\frac{\partial w_i}{\partial Y} - d_{11}\frac{\partial \phi_i}{\partial Y}\right) = 0 \tag{10}$$

where $\nabla^2 = \partial^2/\partial X^2 + \partial^2/\partial Y^2$.

From Li and Mataga [9], a new function ψ is introduced as follows:

$$\psi_i = \phi_i - \frac{e_{15}^0}{d_{11}^0} w_i \tag{11}$$

By substituting Eq. (11) for Eqs. (9) and (10), the dynamic governing equations are transformed into the following equations:

$$\nabla^2 w_i + \beta \frac{\partial w_i}{\partial Y} = \frac{1}{c_2^2} \frac{\partial^2 w_i}{\partial t^2} \tag{12}$$

$$\nabla^2 \psi_i + \beta \frac{\partial \psi_i}{\partial Y} = 0 \tag{13}$$

where

$$c_2 = \sqrt{\mu_0 / \rho_0} \ , \ \mu_0 = c_{44}^0 + (e_{15}^0)^2 / d_{11}^0 \tag{14}$$

For the problem of a moving crack with constant velocity "v" along the X-direction, it is convenient to introduce a Galilean transformation such as

$$x = X - vt \ , \ y = Y \ , \ z = Z \ , \ t = t \tag{15}$$

where (x, y, z) is the translating coordinate system attached to the center of the moving crack.

In the transformed coordinate system, the dynamic anti-plane governing equations for piezoelectric materials can be simplified to the following forms:

$$\alpha^2 \frac{\partial^2 w_i(x,y)}{\partial x^2} + \frac{\partial^2 w_i(x,y)}{\partial y^2} + \beta \frac{\partial w_i(x,y)}{\partial y} = 0 \tag{16}$$

$$\nabla^2 \psi_i(x,y) + \beta \frac{\partial \psi_i(x,y)}{\partial y} = 0 \tag{17}$$

where

$$\alpha = \sqrt{1 - (v / c_2)^2} \tag{18}$$

A Fourier transform is applied to Eqs. (16) and (17), and the results are as follows:

$$w_i(x,y) = \frac{2}{\pi} \int_0^\infty \left[A_{1i}(s) e^{-q_1 y} + A_{2i}(s) e^{q_2 y} \right] \cos(sx) ds \tag{19}$$

$$\phi_i(x,y) = \frac{2}{\pi} \frac{e_{15}^0}{d_{11}^0} \int_0^\infty \left[A_{1i}(s) e^{-q_1 y} + A_{2i}(s) e^{q_2 y} \right] \cos(sx) ds + \frac{2}{\pi} \int_0^\infty \left[B_{1i}(s) e^{-p_1 y} + B_{2i}(s) e^{p_2 y} \right] \cos(sx) ds \tag{20}$$

where

$$q_1 = \delta + \frac{\beta}{2} \ , \ q_2 = \delta - \frac{\beta}{2} \tag{21}$$

$$p_1 = \lambda + \frac{\beta}{2} \ , \ p_2 = \lambda - \frac{\beta}{2} \tag{22}$$

$$\delta = \sqrt{\alpha^2 s^2 + \frac{\beta^2}{4}} \ , \ \lambda = \sqrt{s^2 + \frac{\beta^2}{4}} \tag{23}$$

A_{ji} and B_{ji} are the unknowns to be solved.

By substituting Eqs. (19) and (20) for Eqs. (7) and (8), we have the following:

$$\sigma_{yzi}(x,y) = \mu_0 \frac{2}{\pi} \int_0^\infty \left[-q_1 A_{1i}(s) e^{-q_2 y} + q_2 A_{2i}(s) e^{q_1 y} \right] \cos(sx) ds + e_{15}^0 \frac{2}{\pi} \int_0^\infty \left[-p_1 B_{1i}(s) e^{-p_2 y} + p_2 B_{2i}(s) e^{p_1 y} \right] \cos(sx) ds \tag{24}$$

$$D_{yi}(x,y) = -d_{11}^0 \frac{2}{\pi} \int_0^\infty \left[p_1 B_{1i}(s) e^{-p_2 y} + p_2 B_{2i}(s) e^{p_1 y} \right] \cos(sx) ds \tag{25}$$

The boundary conditions can be written as

$$\sigma_{yzi}(x,0) = -\tau_0 \ , \ (0 \le x < a) \tag{26}$$

$$w_1(x,0^+) = w_2(x,0^-) \ , \ (a < x \le \infty) \tag{27}$$

$$D_{yi}(x,0) = -D_0 \ , \ (0 \le x < a) \tag{28}$$

$$\phi_1(x,0^+) = \phi_2(x,0^-) \ , \ (a < x \le \infty) \tag{29}$$

$$\sigma_{yz1}(x,0^+) = \sigma_{yz2}(x,0^-) \ , \ (a < x \le \infty) \tag{30}$$

$$D_{y1}(x,0^+) = D_{y2}(x,0^-) \ , \ (a < x \le \infty) \tag{31}$$

$$E_{x1}(x,0^+) = E_{x2}(x,0^-) \ , \ (a < x \le \infty) \tag{32}$$

$$\sigma_{yz1}(x,h_1) = \sigma_{yz2}(x,-h_2) = 0 \ , \ (0 < x \le \infty) \tag{33}$$

$$D_{y1}(x,h_1) = D_{y2}(x,-h_2) = 0 \ , \ (0 < x \le \infty) \tag{34}$$

where τ_0 and D_0 are the uniform shear traction and electric displacement, respectively.

By applying the edge loading conditions of Eqs. (33) and (34), the unknowns in Eqs. (24) and (25) are evaluated as follows:

$$-q_1 A_{11}(s) e^{-q_2 h_1} + q_2 A_{21}(s) e^{q_1 h_1} = 0 \ ,$$
$$-q_1 A_{12}(s) e^{q_2 h_2} + q_2 A_{22}(s) e^{-q_1 h_2} = 0 \tag{35}$$

$$-p_1 B_{11}(s) e^{-p_2 h_1} + p_2 B_{21}(s) e^{p_1 h_1} = 0 \ ,$$
$$-p_1 B_{12}(s) e^{p_2 h_2} + p_2 B_{22}(s) e^{-p_1 h_2} = 0 \tag{36}$$

The continuity conditions of Eqs. (30) and (31) lead to the following relations between the unknowns:

$$q_1\left(A_{11}(s)-A_{12}(s)\right)=q_2\left(A_{21}(s)-A_{22}(s)\right) \tag{37}$$
$$p_1\left(B_{11}(s)-B_{12}(s)\right)=p_2\left(B_{21}(s)-B_{22}(s)\right) \tag{38}$$

It is convenient to use the following definitions:

$$A_{11}(s)-A_{12}(s)+A_{21}(s)-A_{22}(s)=A(s) \tag{39}$$
$$B_{11}(s)-B_{12}(s)+B_{21}(s)-B_{22}(s)=B(s) \tag{40}$$

Using Eqs. (35) to (40), we can obtain the following relations:

$$A_{11}(s)=\frac{1-e^{-2\delta h_2}}{(k+1)(1-e^{-4\delta h})}A(s) \tag{41}$$
$$A_{12}(s)=\frac{-e^{-2\delta h_2}(1-e^{-2\delta h_1})}{(k+1)(1-e^{-4\delta h})}A(s) \tag{42}$$
$$A_{21}(s)=\frac{k\,e^{-2\delta h_1}(1-e^{-2\delta h_2})}{(k+1)(1-e^{-4\delta h})}A(s) \tag{43}$$
$$A_{22}(s)=\frac{-k(1-e^{-2\delta h_1})}{(k+1)(1-e^{-4\delta h})}A(s) \tag{44}$$
$$B_{11}(s)=\frac{1-e^{-2\lambda h_2}}{(f+1)(1-e^{-4\lambda h})}B(s) \tag{45}$$
$$B_{12}(s)=\frac{-e^{-2\lambda h_2}(1-e^{-2\lambda h_1})}{(f+1)(1-e^{-4\lambda h})}B(s) \tag{46}$$
$$B_{21}(s)=\frac{f\,e^{-2\lambda h_1}(1-e^{-2\lambda h_2})}{(f+1)(1-e^{-4\lambda h})}B(s) \tag{47}$$
$$B_{22}(s)=\frac{-f(1-e^{-2\lambda h_1})}{(f+1)(1-e^{-4\lambda h})}B(s) \tag{48}$$

where

$$k=\frac{q_1}{q_2}\ ,\quad f=\frac{p_1}{p_2}\ ,\quad h=h_1+h_2 \tag{49}$$

Eq. (32) leads to the following relation:

$$B(s)=-\frac{e_{15}^0}{d_{11}^0}A(s) \tag{50}$$

The two mixed boundary conditions of Eqs. (26) to (29) lead to dual integral equations in the following forms:

$$\int_0^\infty s\,F(s)\,A(s)\cos(sx)ds=\frac{\pi}{2}\frac{\tau_0}{\gamma}\quad (0\le x<a)$$

$$\int_0^\infty A(s)\cos(sx)\,ds=0\quad (a<x\le\infty) \tag{51}$$

where

$$F(s)=\frac{\pi}{2}\frac{1}{\gamma}\left[\mu_0\frac{q_1}{k+1}\frac{(1-e^{-2\delta h_1})(1-e^{-2\delta h_2})}{1-e^{-4\delta h}}-\frac{\left(e_{15}^0\right)^2}{d_{11}^0}\frac{p_1}{f+1}\frac{(1-e^{-2\lambda h_1})(1-e^{-2\lambda h_2})}{1-e^{-4\lambda h}}\right] \tag{52}$$

$$\gamma=\frac{1}{2}\left(\mu_0\alpha-\frac{\left(e_{15}^0\right)^2}{d_{11}^0}\right) \tag{53}$$

The set of dual integral Eq. (51) may be solved by using the new function $\Omega(\xi)$ (Sih [10]) defined by

$$A(s)=\int\xi\,\Omega(\xi)J_0(s\xi)\,d\xi \tag{54}$$

where J_0 is the zero-order Bessel function of the first kind.

By inserting Eq. (54) into Eq. (51), we can find that the auxiliary function $\Omega(\xi)$ is given by the Fredholm integral equation of the second kind in the following form:

$$\Omega(\xi)+\int_0^a K(\xi,\eta)\,\Omega(\eta)\,d\eta=\frac{\pi}{2}\frac{\tau_0}{\gamma} \tag{55}$$

where

$$K(\xi,\eta)=\eta\int_0^\infty s\left[F(s)-1\right]J_0(s\eta)J_0(s\xi)\,ds \tag{56}$$

We introduce the following dimensionless variables and functions for numerical analysis:

$$s=\frac{S}{a},\ \beta=\frac{\mathrm{B}}{a},\ \delta=\frac{\Delta}{a},\ \lambda=\frac{\Lambda}{a} \tag{57}$$
$$\eta=a\mathrm{H}\ ,\quad \xi=a\Xi \tag{58}$$
$$\Omega(\xi)=\frac{\pi}{2}\frac{\tau_0}{\gamma}\frac{\Psi(\Xi)}{\sqrt{\Xi}} \tag{59}$$

By substituting Eqs. (57) to (59) for Eqs. (55) and (56), we can obtain the Fredholm integral equation of the second kind in the following form:

$$\Psi(\Xi)+\int_0^1 L(\Xi,\mathrm{H})\,\Psi(\mathrm{H})\,d\mathrm{H}=\sqrt{\Xi} \tag{60}$$

where

$$L(\Xi,\mathrm{H})=\sqrt{\Xi\mathrm{H}}\int_0^\infty S\left[F\left(\frac{S}{a}\right)-1\right]J_0(S\mathrm{H})J_0(S\Xi)dS \quad (61)$$

$$F\left(\frac{S}{a}\right)=\frac{1}{S}\frac{1}{\gamma}\left[\mu_0\frac{Q_1}{k+1}\frac{(1-e^{-2\Delta\left(\frac{h}{a}+\frac{e}{a}\right)})(1-e^{-2\Delta\left(\frac{h}{a}-\frac{e}{a}\right)})}{1-e^{-4\Delta\frac{h}{a}}}\right. \quad (62)$$
$$\left.-\frac{\left(e_{15}^0\right)^2}{d_{11}^0}\frac{P_1}{f+1}\frac{(1-e^{-2\Lambda\left(\frac{h}{a}+\frac{e}{a}\right)})(1-e^{-2\Lambda\left(\frac{h}{a}-\frac{e}{a}\right)})}{1-e^{-4\Lambda\frac{h}{a}}}\right]$$

$$Q_1=\Delta+\frac{\mathrm{B}}{2}\ ,\ P_1=\Lambda+\frac{\mathrm{B}}{2} \quad (63)$$

e denotes the eccentricity.

The mode III dynamic stress intensity factor $K_{III}^{\tau}(v)$ is defined and determined in the following form:

$$K_{III}^{\tau}(v)=\tau_0\sqrt{\pi a}\,\Psi(1) \quad (64)$$

in which the function $\Psi(1)$ can be calculated from Eq. (60).

3. Discussions

3.1 Case study

The static solution ($v=0$ or $\alpha=1$) can be derived from Eq. (60). In this case, the kernel function $L(\Xi,\mathrm{H})$ can be obtained as

$$\Psi(\Xi)+\int_0^1 L(\Xi,\mathrm{H})\Psi(\mathrm{H})\,d\mathrm{H}=\sqrt{\Xi} \quad (65)$$

where

$$F\left(\frac{S}{a}\right)=\frac{1}{S}\frac{2Q_1}{k+1}\frac{\left(1-e^{-2\Lambda\left(\frac{h}{a}+\frac{e}{a}\right)}\right)\left(1-e^{-2\Lambda\left(\frac{h}{a}-\frac{e}{a}\right)}\right)}{1-e^{-4\Lambda\frac{h}{a}}} \quad (66)$$

Eq. (65) is the same as that of Shin and Kim (2003).

3.2 Numerical results of the dynamic stress intensity factor

To investigate the effect of the gradient of material properties, crack moving velocity, and eccentricity of the crack on the stress intensity factor, a numerical analysis is carried out. We assume that the piezoelectric material properties at $y=0$ are same as PZT-5H, which are listed in Table 1. N, C and V are the force in Newtons, charge in coulombs, and electric potential in volts, respectively.

Fig. 2 displays the variation of the normalized dynamic stress intensity factor (DSIF) $K_{III}(v)/\tau_0\sqrt{\pi a}$ against the normalized crack length a/h with various B values at $e/h=0.4$ and $v/c_2=0.2$. The DSIF in FGPM increases when the crack length and the material property gradient increase.

Fig. 3 shows the variation of the normalized DSIF against normalized crack length with various crack locations at $B=2.0$ and $v/c_2=0.2$. In this case, the DSIF in FGPM increases as eccentricity of the crack location increases. The effect of the crack mov-

Table 1. Material properties of piezoelectric ceramic at $y=0$.

Material Properties	Symbol	Unit	Piezo-ceramics
Elastic Stiffness	c_{44}^0	$\times10^{10}\ N/m^2$	2.3
Piezoelectric Constant	e_{15}^0	C/m^2	17.0
Permittivity	d_{11}^0	$\times10^{-10}\ C/V\,m$	150.4

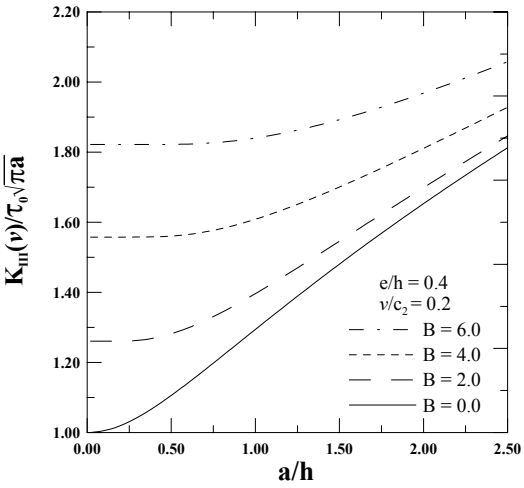

Fig. 2. Stress intensity factor $K_{III}(v)/\tau_0\sqrt{\pi a}$ versus a/h with various values of B at $e/h=0.4$ and $v/c_2=0.2$.

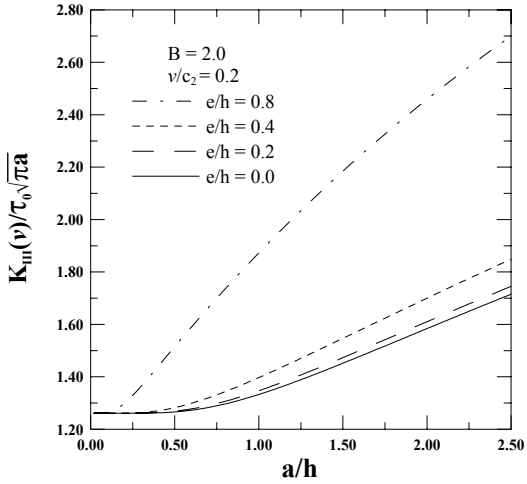

Fig. 3. Stress intensity factor $K_{III}(v)/\tau_0\sqrt{\pi a}$ versus a/h with various values of e/h at $B=2.0$ and $v/c_2=0.2$.

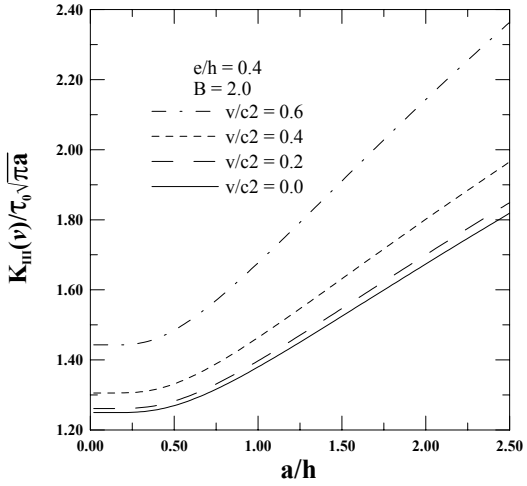

Fig. 4. Stress intensity factor $K_{III}(v)/\tau_0\sqrt{\pi a}$ versus a/h with various values of v/c_2 at $e/h=0.4$ and $B=2.0$.

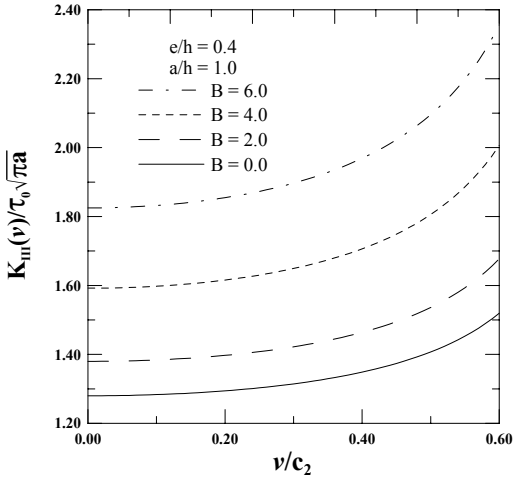

Fig. 5. Stress intensity factor $K_{III}(v)/\tau_0\sqrt{\pi a}$ versus v/c_2 with various values of B at $e/h=0.4$ and $a/h=1.0$.

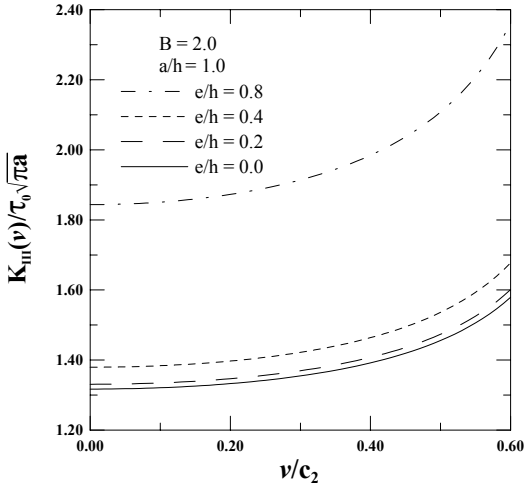

Fig. 6. Stress intensity factor $K_{III}(v)/\tau_0\sqrt{\pi a}$ versus v/c_2 with various values of e/h at $B=2.0$ and $a/h=1.0$.

ing velocity on the variation of the normalized DSIF in FGPM is shown in Fig. 4. The DSIF in FGPM increases with the increase of the crack moving velocity. Particularly from Figs. 2 to 4, the DSIF in FGPM always increases with the increase of the crack length whatever values the non-homogeneous material constant, eccentricity of crack length, and the crack moving velocity have.

Figs. 5 and 6 show the variation of the normalized DSIF in FGPM against normalized crack moving velocity. The DSIF in FGPM grows rapidly as the crack moving velocity increases regardless of the material property gradient and eccentricity of crack location. We also determined that the increase in the crack moving velocity significantly affects the variation of the DSIF in FGPM when the material property gradient and eccentricity of the crack location have larger values. As seen in Figs. 3 and 6, the DSIF in FGPM increases more rapidly as the crack moves to the strip surface more closely.

4. Conclusions

The electroelastic problem of a moving eccentric

crack off the center line in a functionally graded piezoelectric ceramic strip under anti-plane shear and in-plane electric loading is analyzed using the integral transform approach. The properties and mass density of the FGPM vary continuously along the thickness. The impermeable crack boundary condition is adopted. The Fredholm integral equations are solved numerically. The computed results show that the normalized DSIF of a moving crack in FGPM increases when the crack moving velocity, eccentricity of crack location, material property gradient, and crack length increase. Particularly, as the crack moving velocity increases, the DSIF in FGPM grows more rapidly. Furthermore, when the material property gradient and eccentricity of crack location have larger values, the increase in the crack moving velocity significantly affects the variation of the DSIF in FGPM.

Acknowledgement

This study was supported by the KHP Dual-Use Component Development Program funded by the Ministry of Knowledge Economy, Republic of Korea.

References

[1] C. Li and G. J. Weng, Antiplane Crack Problem in Functionally Graded Piezoelectric Materials, *ASME J. Appl. Mech.* 69 (2002) 481-488.

[2] J. W. Shin and T. U. Kim, Functionally Graded Piezoelectric Strip with Eccentric Crack under Anti-plane Shear, *KSME Int. J.* 17 (6) (2003) 854-859.

[3] J. W. Shin, T. U. Kim and S. C. Kim, Dynamic Characteristics of an Eccentric Crack in a Functionally Graded Piezoelectric Ceramic Strip, *KSME Int. J.* 18 (9) (2004) 1582-1589.

[4] B. Jin and Z. Zhong, A Moving Mode-III Crack in Functionally Graded Piezoelectric Material : Permeable Problem, *Mech. Res. Commun.* 29 (2002) 217-224.

[5] B. Jin, A. K. Soh and Z. Zhong, Propagation of an Anti-Plane Moving Crack in a Functionally Graded Piezoelectric Strip, *Arch. Appl. Mech.* 73 (3) (2003) 252-260.

[6] S. M. Kwon, On the Dynamic Propagation of an Anti-plane Shear Crack in a Functionally Graded Piezoelectric Strip, *Acta Mech.* 167 (1-2) (2004) 73-89.

[7] K. Hu and Z. Zhong, A Moving Mode-III Crack in a Functionally Graded Piezoelectric Strip, *Int. J. Mech. Mater. Des.* 2 (1) (2005) 61-79.

[8] F. Erdogan, The Crack Problem for Bonded Nonhomogeneous Materials under Antiplane Shear Loading, *ASME J. Appl. Mech.* 52 (1985) 823-828.

[9] S. Li and P. A. Mataga, Dynamic Crack Propagation in Piezoelectric Materials-Part I. Electrode Solution, *J. Mech. Phys. Solids* 44 (1996) 1799-1830.

[10] G. C. Sih, *Mechanics of fracture 1 - Methods of analysis and solutions of crack problems*, Noordhoff International Publishing, Leyden, Netherlands, (1973).

Jeong Woo Shin received a B.S. and M.S. degree in Mechanical Engineering from Yonsei University in Seoul, Korea in 1998 and 2000, respectively. A major field of Mr. Shin is fracture mechanics. He is currently working on the KARI (Korea Aerospace Research Institute) as a senior researcher. He conducted load analysis of fixed wing aircraft and full scale airframe static test at the KARI. He is now developing landing gear in the KHP (Korea Helicopter Program) as a performance engineer.